Desalination and Water Treatment
www.deswater.com

doi: 10.5004/dwt.2022.28037

247 (2022) 92–99
January

Photocatalytic degradation of nitrotoluene in synthetic wastewater by $CoFe_2O_4/SiO_2/TiO_2$ nanoparticles using Box–Behnken experimental design

Aref Shokri

Jundi-Shapur Research Institute, Dezful, Iran, email: aref.shokri3@gmail.com

Received 5 September 2021; Accepted 4 December 2021

ABSTRACT

The release of nitrotoluene (NT) to aqueous media results in a solemn problem in water resources because of harmfulness and its potential carcinogenicity. In this study, the degradation of NT was explored by synthesized $CoFe_2O_4/TiO_2/SiO_2$ nano-photocatalyst. The characterization of catalyst was determined using X-ray diffraction (XRD), energy scattering X-ray spectroscopy (EDX), Fourier transform infrared spectroscopy (FTIR), and transmission electron microscopy (TEM). The Box–Behnken design of experiment was used to study the influence of three sovereign parameters on the response to acquire the optimal conditions. The analysis of variance (ANOVA) was executed to regulate the significance of the influences of independent factors on the response. The effect of various operational parameters on the degradation efficacy such as solution pH, catalyst dosage and initial NT concentration was investigated. Also, increasing NT concentration results in the formation of degradation intermediates that may be adsorbed on the catalyst surface and inactivate the active sites and too much catalyst leads to accumulation, which leads to a reduction in photocatalyst efficiency based on a decrease in the amounts of active sites of the catalyst. At optimum conditions (25 mg/L of NT, catalyst concentration of 1.03 g/L, and pH at 4) and after 150 min of reaction, the NT and COD removal were 97.8% and 60.7%, respectively. This nano-photocatalyst was influential in removing NT, but it can eliminate the COD to some extent.

Keywords: Photocatalytic degradation; $CoFe_2O_4/SiO_2/TiO_2$; Box–Behnken experimental design; Nitrotoluene; Wastewater treatment

1. Introduction

Many systems involving textiles, pesticides, and paper manufacturing industries consume nitroaromatics, which are dangerous to the environment and humans if released into the water without treatment. One of the common nitroaromatics is p-nitrotoluene and studies displayed that it is suspicious in hormone disruption [1]. Thus, some researches have been devoted degrading the PNT in wastewater [2,3]. NT is a severe risk to human health and many ecosystems due to its poisonousness and causing cancers. The United States Environmental Protection Agency (EPA) identified NT as a priority pollutant [4]. Therefore, employing an effective and economical method to eliminate or reduce NT has been investigated.

Overactive adsorption followed by the burning of carbon is operative expertise to eliminate NT in an aqueous environment. But this technique requires high temperatures and it is costly because of the high carbon requirement and raises anxieties about the air quality created by combustion [5]. Also, the NT pollutant has been treatment by biological methods [6]. It is hard to comply with the EPA discharge range with the NT aerobic biological industrial application [5].

There are various methods for the treatment of pollutants [7–9]. In current decades, advanced oxidative processes (AOPs) have been used as an alternate to NT degradation in aqueous solutions [10,11]. In these methods, high reactive hydroxyl radicals were produced to oxidize pollutants and change them to safe products including, CO_2 and H_2O [11,12]. The photocatalysts are a branch of AOPs which has been used for the degradation of toxic pollutants in aqueous media due to their economic, lower usage of reagents and materials, and high performance [13]. TiO_2 is one of the most proficient photocatalysts which is used for the treatment of wastewater based on its high stability and non-toxic efficacy [14], low cost [15], good electrical and thermal conductivity [16], high reaction and chemical inactivity [17]. The separation and recycling of TiO_2 from remediated wastewater are the main challenge in the industrial application of TiO_2 nanoparticles and often, it is a complex process and energy consumer [18].

To solve these difficulties, many works have been done to design the photocatalytic process. For example, by combining magnetic components and TiO_2-based photocatalysts, the problem can be solved to some extent. The magnetic photocatalysts are simply separated from an aqueous environment utilizing an exterior magnetic field [19]. However, straight contact between the magnetic core and the shell of TiO_2 might lead to charge transporters from the titanium shell to the core of iron oxide and then iron ions were leached from the catalyst structure into an aqueous environment [20]. In this regard, introducing a passive intermediate layer of silica can prevent the destruction and dissolution of magnetic nuclei and reduce photocatalytic activity by dropping the negative effect of magnetic oxide centers on TiO_2 photocatalyst [21]. The TiO_2 nanoparticles were used by Saien et al. as an operative photocatalyst for the degradation of organic contaminants in the actual effluents of the Iranian refinery and about 78% of COD was removed under pH of 3, at a low catalyst concentration, the temperature at 45°C, and 120 min of reaction [22].

In the present study, $CoFe_2O_4/TiO_2/SiO_2$ nanoparticles with core-shell were manufactured by a three-step process and then it was used as a photocatalyst to decompose NT in an aqueous solution under ultraviolet radiation. As far as the author searched, no study has evaluated the degradation of NT by $CoFe_2O_4/TiO_2/SiO_2$ particles. The dependency of the removal efficacy on the operative variables such as the pH of the solution, the catalyst doses and the initial concentration of the NT, was considered using the Box–Behnken design method.

2. Experimental

2.1. Materials

Ferric nitrate nonahydrate [$Fe(NO_3)_3{\cdot}9H_2O$], cobalt nitrate hexahydrate [$Co(NO_3)_2{\cdot}6H_2O$], cetyltrimethylammonium bromide (CTAB), sodium hydroxide (NaOH), tetraethyl orthosilicate (TEOS), titanium (IV) butoxide, citric acid, and ammonium hydroxide (NH_4OH) were supplied from Sigma-Aldrich. The NT and ethanol were purchased from Merck. In all the experiments, deionized water was used. All chemicals were applied, deprived of additional purification.

2.2. Preparation of $CoFe_2O_4$ nanocatalyst

The nanoparticles of $CoFe_2O_4$ were synthesized with some change based on the method presented by some researchers [23]. Using 250 mL of RBF, 1 g $Co(NO_3)_2{\cdot}6H_2O$ and 0.8 g $Fe(NO_3)_3{\cdot}9H_2O$ was dissolved in 150 ml distilled water and 15 ml of deionized water containing 1 M CTAB was unhurriedly added to this solution. Later, the solution of sodium hydroxide was added to the mixture by droplet, until the pH was taking 11. At that time, immediately the precipitation happened and the color of solution was changed into shadowy brown. The magnetic separation was used for the collection of the subsequent precipitation and it was washed until the pH was neutral. Then by applying a Schlenk line and using rotary evaporation and drying below a vacuum, the water was eliminated.

2.3. Preparation of $CoFe_2O_4/SiO_2$ nanoparticles

The nanoparticles of $CoFe_2O_4/SiO_2$ were synthesized according to the Green et al. [24] method with slight changes. 3 g acid citric was added to 50 ml of distilled water and 100 mL ethanol. Then, 0.05 g of $CoFe_2O_4$ nanoparticles were added to the mixture. The blend was homogenized by sonication for 5 min. Then, about 0.7 mL of TEOS solution was added to the subsequent solution, and again sonicated for 15 min. Later, by adding 25 mL of hydroxide ammonium, the solution was stirred by sonication in ice for 50 min. Then, the acquired samples were separated using centrifuging, washing by ethanol and formerly drying thru rotary evaporation.

2.4. Synthesize of $CoFe_2O_4/TiO_2/SiO_2$ nanoparticles

The method reported by other researchers [25] with a bit of change was used to synthesize $CoFe_2O_4/TiO_2/SiO_2$ nanoparticles. About 0.7 g of $CoFe_2O_4/SiO_2$ particles in 100 mL of ethanol was dispersed around the bottom flask and sonicated for 15 min in ice. Then, the addition of 0.5 mL of titanium tetra butoxide was stirred in ice for an alternative 15 min. The blend was agitated at 60°C at 3 h. The acquired product was collected through centrifuge and washed with ethanol. Lastly, the rotary evaporation was used for moisture removal from $CoFe_2O_4/TiO_2/SiO_2$ structure and finally, it was calcinated at 400°C for 2 h.

2.5. Characterization of the prepared nanoparticle

The crystal phases and structure were considered by an XRD (X'PERT PRO MPD, Panalytical) utilizing a graphite monochromatic Cu-Kα radiation at 30 mA current and 40 kV voltage. The EDX test was applied to recognize the elemental conformation of nanoparticles. A TEM, EM 208S, Philips 100 kV was applied to detect the size, morphology of the surface, and the structure of the produced particles. The FT-IR spectra were logged utilizing the FT-IR, Burcher Tensor 27, in the variety between 500 to 4,000 cm^{-1}. The pH of zero-point charges (pH_{ZPC}) of $CoFe_2O_4/TiO_2/SiO_2$ was determined by applying an electrolyte solution (0.01 M NaCl).

2.6. Photoreactor and procedure

All experiments were accomplished in a glass reactor with one liter of volume and furnished with a sampling

arrangement (Fig. 1). A 15-watt Philips mercury lamp (UV-C) was positioned in the center of the reactor vertically as a light spring and a quartz tube was used to guard the lamp. Also, an air pump was applied to inter the oxygen to the reactor (not shown in Fig. 1) and ensure the aerobic conditions required for photocatalysis. The reactor had an external flow water jacket measured by a thermostat to control the temperature fixed at 25°C by a water bath (BW 20G) made by a Korean company. Mix the solution with a mixer until the solution is homogeneous. The initial solution pH was attuned by a pH meter (PT-10P Sartorius Instrument) from the German Company.

For each test, an identified quantity of catalyst was added to the synthetic wastewater containing NT at definite concentrations and the suspension pH was attuned with H_2SO_4 or KOH (0.1 M) as needed. The mix was stirred for 30 min in the dark to balance the NT adsorption on the catalyst surface. The mixture of catalyst and a watery solution containing pollutant was poured into a reactor and irradiated by ultraviolet light for 150 min. After a specific time, samples were taken and the catalyst particles were separated from suspension. The final concentration of NT was then determined by a spectrophotometer (Agilent 5443).

The COD removal percent was measured by spectrophotometer (Hach, DR 5000, USA Jenway) at 600nm employing standard procedures [26]. The time of reaction was 150 min in all tests. The removal of NT was gained thru the resulting Eq. (1):

$$\text{Removal of NT}(\%) = \left(\frac{\text{NT}_0 - \text{NT}_t}{\text{NT}_0}\right) \times 100 \quad (1)$$

where NT_0 and NT_t are NT values at the preliminary and t times, respectively.

2.7. Statistical analysis and design of experiment

The design of experiment was applied for the optimization of NT removal scientifically. The effects of NT concentration (C_{HP}), Catalyst concentration (C_{Cat}), and acidity (pH) on NT removal were studied. Table 1 shows the input variables (C_{NT}, C_{Cat} and pH) with their levels.

3. Results and discussion

3.1. Characterization of materials

The XRD spectra of $CoFe_2O_4/TiO_2/SiO_2$ nanoparticles are illustrated in Fig. 2. The peaks at 30.0, 44.0, 35.0, 63.0 and 57.0 were related to the distinctive diffraction peaks of the cubic spine phase based on the standard $CoFe_2O_4$ XRD (Card NO. 22-1086, JCPDS) [24]. In the XRD spectrum of $CoFe_2O_4/SiO_2/TiO_2$, the peaks detected at 70.0, 54.0 and 27.0 are associated with the rutile. However, the peaks at angles 25, 40, 48.0, 52, 54.0, 70 and 78.0 are associated with the anatase phase of TiO_2. These results agreed with the anatase standard XRD spectrums (Card No.76-1940, JCPDS) and TiO_2 in

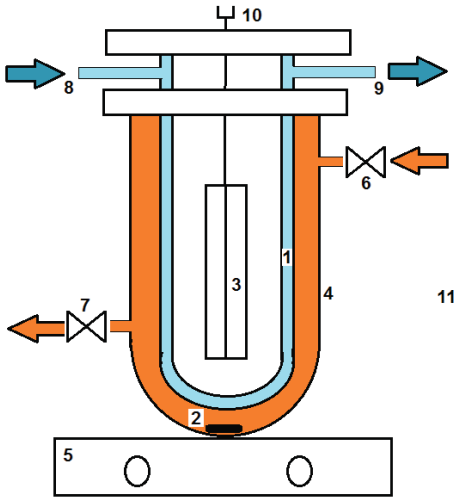

Fig. 1. Schematic of the experimental setup in laboratory: (1) Jacket of cooling water, (2) Stirring bar, (3) Light source, (4) Reactor, (5) Stirrer, (6) Entrance of reactor, (7) Output of reactor, (8) Input of cooling water, (9) Output of cooling water, (10) Electric linking, (11) Insulated box.

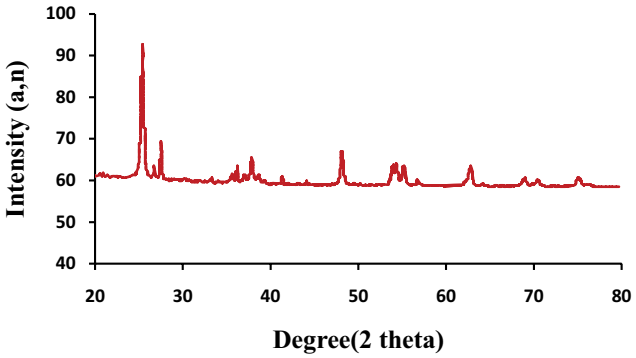

Fig. 2. XRD spectra pattern of $CoFe_2O_4/SiO_2/TiO_2$.

Table 1
The levels of experimental variables

Variable	Levels and Range		
	Low (–1)	Middle (0)	High (+1)
Initial concentration of NT, C_{NT} (mg/L)	25	50	75
Catalyst concentration, C_{Cat} (g/L)	0.25	0.75	1.25
pH	4	7	10

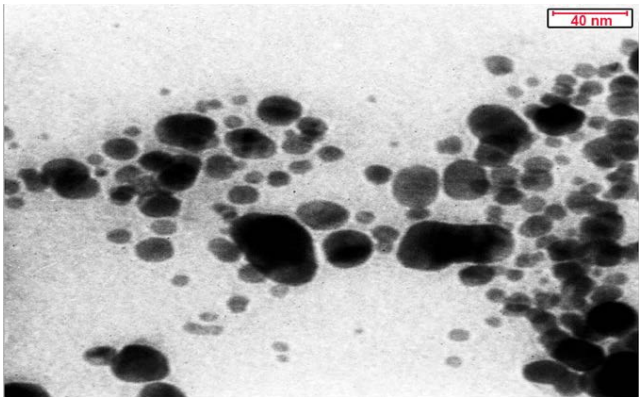

Fig. 3. TEM images of $CoFe_2O_4/SiO_2/TiO_2$.

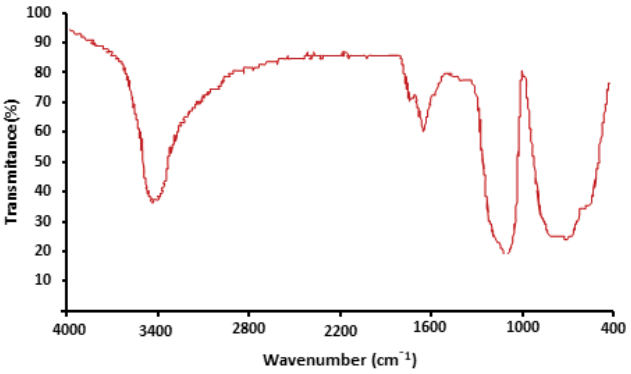

Fig. 4. FTIR spectra of $CoFe_2O_4/SiO_2/TiO_2$.

the rutile phase (Card number 89-4203, JCPDS) phase. The most intense diffraction peak for $CoFe_2O_4$ (35) and the SiO_2 peak (2θ = 15–25) converted frailer in the $CoFe_2O_4/TiO_2/SiO_2$ XRD spectrum, based on the creation of TiO_2 coating [27]. These results were approved by Sabar et al. [28].

The EDX result exhibits the presence of elements such as oxygen (O), carbon (C), iron (Fe), titanium (Ti), silicon (Si), and cobalt (Co) in the structure of $CoFe_2O_4/SiO_2/TiO_2$. Ti and O were the main elements in the synthesis course with 39 and 44.5 wt%, respectively. Furthermore, in the EDX spectrum, the peaks originated from impurities were not detected, and this subject can confirm the high purity of the manufactured catalyst.

Fig. 3 displays the spherical structures of $CoFe_2O_4/TiO_2/SiO_2$ nanoparticles with an average size between 40 to 60 nm. But the existence of the TiO_2 layer in the structure of $CoFe_2O_4/SiO_2$ was not displayed fine. However, the EDX and XRD outcomes proposed that on the surfaces of $CoFe_2O_4/SiO_2$ nanoparticles the TiO_2 layer was coated. According to the mentioned results along with TEM images, the approximate depth of the TiO_2 layer was valued at about 30 nm. Some researchers found that the TEM image of $CoFe_2O_4/SiO_2$ particles was a definite core-shell with a high agglomeration degree according to the magnetic attraction between silica layers and cobalt ferrite [28].

In Fig. 4 the FTIR spectra of prepared samples are demonstrated. The peaks at 1,620 and 3,420 cm^{-1} were associated with the stretch vibration of the H–O–H bending vibration and O–H functional groups of the molecules of water at a free state and adsorbed on the particle surface, respectively. The irregular vibration of Si–O–Si can be identified by a robust peak at 1,100 cm^{-1}. In addition, the vibration of the Si–O–H band can be recognized by a robust peak at 960 cm^{-1} [29]. For $CoFe_2O_4/SiO_2/TiO_2$, the observed peaks at 790 and 712 cm^{-1} can be related to the stretch vibration of Ti–O–Ti in anatase TiO_2 [30]. Through comparison with the FTIR spectra of $CoFe_2O_4/SiO_2$, the strength at 1,090 cm^{-1} related to the irregular vibration of Si–O–Si reduced in the spectrum of $CoFe_2O_4/TiO_2/SiO_2$ based on the coating of TiO_2 on $CoFe_2O_4/SiO_2$ surfaces [31]. Some studies performed by other researchers confirmed the mentioned results [32–34].

3.2. Designing of experiments

The Box–Behnken design of experiment requires a smaller numeral of experiments [26]. Based on the design of experiment, the resulting model was presented for the response (Y), as a polynomial equation of parameters [Eq. (2)]:

$$Y = b_0 + \sum b_i x_i + \sum\sum b_{ij} x_i x_j + \sum\sum b_{ii} x_i^2 + \varepsilon \quad (2)$$

where b_0 is a persistent number, ε is the equation remainder, b_{ij} is a linear interaction between the input variables of x_j and x_i (j = 1,2,3 and i = 1,2,3), the slope of the variable is b_i, and b_{ii} is the second-order of the input variable x_i (i = 1,2,3). Analysis of variance (ANOVA) was used to examine the significance of each variable in the polynomial equation [Eq. (2)] [35]. In the ANOVA, the level of significance or p-value was set at 0.05. The p-values less than 0.0500 elect the importance of model terms. The model terms are not significant with the p-values more than 0.1000. The statistical significance of the second-order models was introduced by the F-value. When the calculated F-value is more than the F-value in table, then the p-value will be much small; it indicates the significance of the model. The calculated F-value is achieved by the ratio of mean squares of regression to the mean squares of residual as the following equation [35]:

$$F\text{-value} = \frac{\mathrm{MS}_{\mathrm{Reg.}}}{\mathrm{MS}_{\mathrm{Res.}}} = \frac{\dfrac{\mathrm{SS}_{\mathrm{Reg.}}}{\mathrm{DF}_{\mathrm{Reg.}}}}{\dfrac{\mathrm{SS}_{\mathrm{Res.}}}{\mathrm{DF}_{\mathrm{Res.}}}} \quad (3)$$

The percentages of NT removal were shown in Table 2 and all tests were performed casually to minimalize the errors of the experiment.

The quadratic relationship was obtained by means of the least squares error technique, to obtain the response in terms of the three independent factors as Eq. (4):

$$\begin{aligned}\text{NT Removal \%} = {} & 73.9 - 0.918X_{\mathrm{NT}} + 120.3X_{\mathrm{Cat}} - 4.44X_{\mathrm{pH}} \\ & + 0.00351X_{\mathrm{NT}}^2 - 52.63X_{\mathrm{Cat}}^2 + 0.138X_{\mathrm{pH}}^2 - 0.088X_{\mathrm{NT}}X_{\mathrm{Cat}} \\ & + 0.0207X_{\mathrm{NT}}X_{\mathrm{pH}} - 2.2X_{\mathrm{Cat}}X_{\mathrm{pH}}\end{aligned} \quad (4)$$

Table 2
Design of experiment for studied variables and their responses at 150 min of reaction

Run no.	Manipulated variables			Responses %
	$X_{C_{NT}}$	$X_{C_{Cat}}$	$X_{C_{pH}}$	
1	75	0.75	10	46.5
2	50	1.25	10	53.0
3	50	0.75	7	65.4
4	50	0.75	7	65.1
5	75	0.25	7	32.9
6	75	0.75	4	65.5
7	75	1.25	7	52.6
8	50	0.25	4	47.3
9	25	0.25	7	54.0
10	50	0.75	7	65.3
11	50	0.25	10	38.5
12	25	0.75	4	94.2
13	50	1.25	4	75.0
14	25	1.25	7	78.1
15	25	0.75	10	69.0

Fig. 5 illustrates the predicted values vs. the observed values of the quadratic model in the removal of NT using Eq. (4).

3.3. Analyzing the variance of the response

As presented in Table 3, the DF for the residual error and the model are 5 and 9, respectively. The model is very significant because the *p*-value is very low. The *p*-value of X_{NT}, X_{Cat}, X_{pH}, and were less than 0.01, which are significant [36]. But, the binary interaction between X_{NT} and X_{pH} has a *p*-value of 0.121 and 0.338 (further than 0.05) which implies that this interaction is non-significant. Additionally, the *p*-value is 0.000 for lack of fit, signifying the fitness of the model.

3.4. Effect of photocatalyst concentration

The tests were carried out to optimize the concentration of the $CoFe_2O_4/TiO_2/SiO_2$ photocatalyst to avoid extra useless catalysts and guarantee the total absorption of efficient photons. The test was performed in catalyst dosage at 0.25–1.25 g/L. The outcomes are shown in Fig. 6. It was clear from the contour plot, by increasing in photocatalyst concentration from 0.25 g/L to about 1 g/L, degradation efficiency improved, which can be related to the enhance in the numeral of active sites on the surface of photocatalyst and subsequently the production of free radicals [36]. At high catalyst amounts, the accessibility of reactive agents on the surface of the catalyst was increased, leading to further degradation of NT [37]. Though, an extra improvement in catalyst concentration to 1.25 mg/L exhibited a reduction in removal proficiency because the turbidity of the solution was increased in high photocatalyst amounts and subsequently the penetration of UV light into the solution was decreased. In addition, too much catalyst leads to accumulation, which leads to a reduction in photocatalyst efficiency based on a decrease in the amounts of active sites of the catalyst [38].

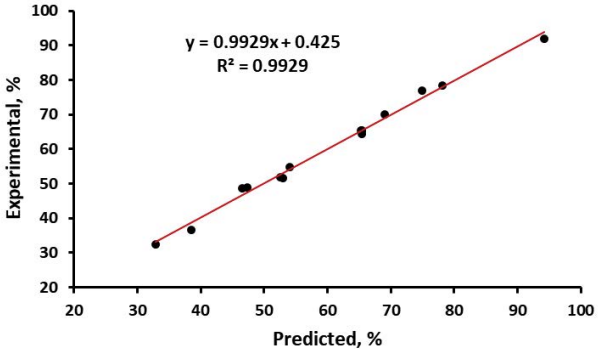

Fig. 5. Comparing the predicted vs. experimental values in NT removal %.

3.5. Effect of initial NT concentration

The influence of the initial concentration of NT on the degradation efficacy was investigated in the range of 25–75 mg/L. As illustrated in Fig. 7, about 25 mg/L of NT is significantly degraded within 150 min of the reaction. It has also been observed that by increasing the initial concentration of NT from 50 to 75 mg/L, the degradation efficiency decreases. Because more NT molecules are adsorbed on the catalyst surface with increasing initial NT concentration, and a notable spread of UV is absorbed by NT molecules compared to photocatalyst particles. Therefore, the penetration of light to the catalyst surface was decreased and accordingly the production of active radicals such as $OH^{\bullet}$ and $O_2^{\bullet-}$ been reduced [39]. Furthermore, increasing NT concentration results in the formation of degradation intermediates that may be adsorbed on the catalyst surface and inactivate the active redox sites, thereby reducing the degradation efficacy.

3.6. Effect of pH

The pH is a significant factor in the photocatalytic application, which impacts the surface charge of the catalyst and the adsorption of contaminants on it [40]. The effect of pH in the degradation of NT using $CoFe_2O_4/TiO_2/SiO_2$ was studied in the range of 4–10. It was clear from Fig. 8, that the degradation efficacy reduced with increasing the pH from 4 to 10. The best effectiveness was attained at pH 4. This phenomenon can be described by the electric charge features of $CoFe_2O_4/TiO_2/SiO_2$ particles and NT molecules. The point of zero charges (pH_{zpc}) of $CoFe_2O_4/TiO_2/SiO_2$ was achieved to be 5.1. Therefore, at the pH below 5.1, the charge of the surface of catalyst was positive whereas at the pH above 5.1, the charge was negative; producing $TiOH_2^+$ and TiO^- species, respectively [Eqs. (5) and (6)] [41]:

$$pH < pH_{zpc} \quad TiOH + H^+ \rightarrow TiOH_2^+ \tag{5}$$

Table 3
ANOVA for the presented model in NT removal %

Source	Adj. SS	DF	Adj. MS	*F*-value	*P*-value
Model	3,573.97	9	397.11	78.12	0.000
Linear	2,823.23	3	941.08	185.13	0.000
X_{NT}	1,195.61	1	1,195.61	235.2	0.000
X_{Cat}	924.5	1	924.5	181.87	0.000
X_{pH}	703.13	1	703.13	138.32	0.000
Square	692.73	3	230.91	45.42	0.000
X^2_{NT}	17.74	1	17.74	3.49	0.121
X^2_{Cat}	639.29	1	639.29	125.76	0.000
X^2_{pH}	5.69	1	5.69	1.12	0.338
2-Way interaction	58.01	3	19.34	3.8	0.092
$X_{NT}X_{Cat}$	4.84	1	4.84	0.95	0.374
$X_{NT}X_{pH}$	9.61	1	9.61	1.89	0.228
$X_{Cat}X_{pH}$	43.56	1	43.56	8.57	0.033
Error	25.42	5	5.08		
Lack of fit	25.41	3	8.47	2,541.000	0.000
Pure error	0.01	2	0.000		
Total	3,599.38	14			

S	R^2	R^2_{adj}	R^2_{pred}
2.25462	99.29%	98.02	88.7%

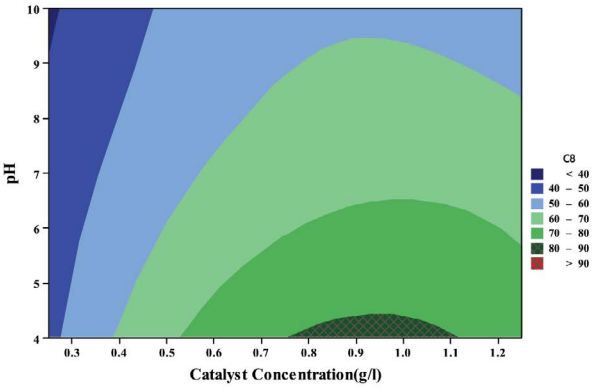

Fig. 6. Influence of catalyst concentration on the removal of NT at 150 min of reaction.

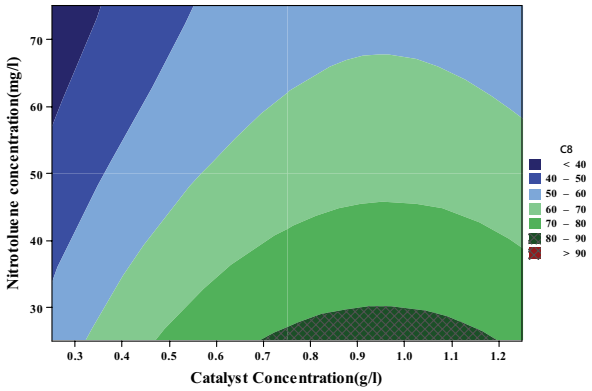

Fig. 7. Effect of NT concentration on photocatalytic efficiency at 150 min of reaction.

$$pH < pH_{zpc} \quad TiOH + OH^- \rightarrow TiO^- + H_2O \tag{6}$$

Thus, the anions of NT with negative charge were quickly adsorbed by the positive charge of $CoFe_2O_4/TiO_2/SiO_2$ surface and afterward, sophisticated photocatalytic efficacy was reached at pH 4. The lowest photocatalytic efficacy at pH 10 may originate from electrostatic repulsion between negatively charged TiO_2 surface and NT anions. Many studies in the literature have reported higher degradation efficiency in the acidic conditions than the other pH values for various organic pollutants [42,43].

The optimum conditions obtained from the software were presented in Table 4. The test was repetitive once again at the predicted optimum conditions and about 97.8% in the removal of NT was achieved after 150 min of reaction. The NT removal percent can increase to 100% with an increase in time. But, 150 min was chosen to consider the changes.

3.7. Mineralization investigation

Through degradation methods, the organic contaminants may be converted to intermediate compounds, which may be more poisonous than the parent pollutant, therefore the mineralization of the whole compound should be investigated. The COD analysis was taken to obtain the degree of NT mineralization under optimal conditions

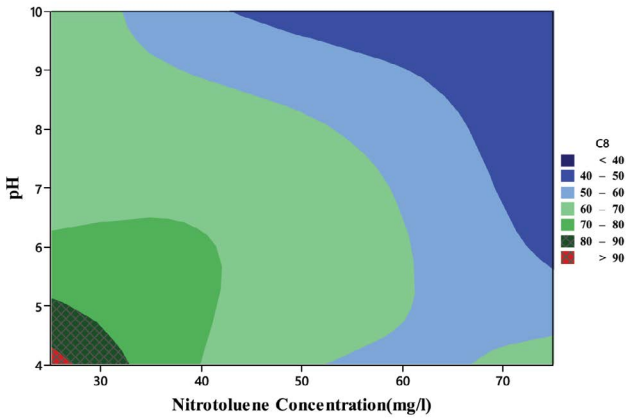

Fig. 8. Influence of solution pH on photo catalytic efficiency at 150 min of reaction.

Table 4
Optimum circumstances in the removal of NT (T = 25°C and t = 150 min)

Parameters	Value
Initial NT concentration, mg/L	25
Catalyst concentration, g/L	1.037
pH	4
Predicted NT removal, %	96.31
Experimental NT removal, %	97.8

and at 150 min of reaction. About 25 mg/L of NT originate 120 mg/L of COD and it was reduced to 35 mg/L. In this study, the NT mineralization reached 60.7% in COD removal, representative of the favorite mineralization was achieved by the $CoFe_2O_4/SiO_2/TiO_2$.

The mineralization efficiency is dependent on the type of photocatalyst, initial concentration of pollutant, chemical structure of pollutant, reaction time and geometry of reactor. For example, recently Fallah et al., [44], published a manuscript on the removal of 2,4-DNT by $CoFe_2O_4/SiO_2/TiO_2$ photocatalyst. The existence of electron withdrawing groups such as "nitro" in the structure of NT or 2,4-DNT, can cause the compound to resist again photocatalytic degradation. This means that the photocatalytic degradation efficiency of 2,4-DNT is lower than NT at the same operational conditions due to the existence of more nitro groups in the molecule structure.

4. Conclusion

In this study, $CoFe_2O_4/TiO_2/SiO_2$ nanoparticles with identified core-shell constructions were synthesized by a simple three-step technique and used as a nano-photocatalyst for the degradation of NT. The characterization of catalyst was determined using XRD, TEM, EDX, and FTIR methods. The effect of various experimental variables on the degradation efficacy such as solution pH, catalyst doses and initial dosage of NT was investigated. The Box–Behnken experimental design was used to study the influences of independent factors on the response to acquire the optimal circumstances. The ANOVA tests were executed to control the significance of the influences of independent factors on the response. The optimization investigation displayed that degradation efficiency reduced with increasing pH, initial NT concentration and extreme photocatalyst loading. The pollutant was converted to intermediate compounds and then to carbon dioxide and water which confirmed by COD removal. The synthesized $CoFe_2O_4/TiO_2/SiO_2$ had an excellent performance in mineralization of NT and at optimum conditions (25 mg/L of NT, catalyst concentration of 1.03 g/L, and pH at 4) and after 150 min, the removal efficacy for NT and COD were 97.8% and 60.7%, respectively.

In conclusion, $CoFe_2O_4/TiO_2/SiO_2$ was an effective catalyst for degradation of NT in an aqueous environment, according to the high degradation efficacy, easy recoverability and proper mineralization.

References

[1] H.R. Pouretedal, Visible photocatalytic activity of co-doped TiO_2/Zr,N nanoparticles in wastewater treatment of nitrotoluene samples, J. Alloys Compd., 735 (2018) 2507–2511.
[2] M. Rostami, H. Mazaheri, A. Hassani Joshaghani, A. Shokri, Using experimental design to optimize the photo-degradation of p-nitro toluene by nano-TiO_2 in synthetic wastewater, Int. J. Eng., 32 (2019) 1074–1081.
[3] M. Rostami, A. Hassani Joshaghani, H. Mazaheri, A. Shokri, Photo-degradation of p-nitro toluene using modified bentonite based nano-TiO_2 photocatalyst in aqueous solution, Int. J. Eng., 34 (2021) 756–762.
[4] G.K.K. Reddy, M. Sarvajith, Y. Nancharaiah, V. Venugopalan, 2,4-Dinitrotoluene removal in aerobic granular biomass sequencing batch reactors, Int. Biodeterior. Biodegrad., 119 (2017) 56–65.
[5] J. Huang, G. Ning, F. Li, G.D. Sheng, Biotransformation of 2,4-dinitrotoluene by obligate marine *Shewanella marisflavi* EP1 under anaerobic conditions, Bioresour. Technol., 180 (2015) 200–206.
[6] D. Kundu, C. Hazra, A. Chaudhari, Biodegradation of 2,4-dinitrotoluene with *Rhodococcus pyridinivorans* NT_2: characteristics, kinetic modeling, physiological responses and metabolic pathway, RSC Adv., 5 (2015) 38818–38829.
[7] A. Azari, R. Nabizadeh, A.H. Mahvi, S. Nasseri, Integrated fuzzy AHP-TOPSIS for selecting the best color removal process using carbon-based adsorbent materials: multicriteria decision making vs. systematic review approaches and modeling of textile wastewater treatment in real conditions, Int. J. Environ. Anal. Chem., (2020) 1–16, doi: 10.1080/03067319.2020.1828395.
[8] A. Azari, M. Yeganeh, M. Gholami, M. Salari, The superior adsorption capacity of 2,4-dinitrophenol under ultrasound-assisted magnetic adsorption system: modeling and process optimization by central composite design, J. Hazard. Mater., 418 (2021) 126348, doi: 10.1016/j.jhazmat.2021.126348
[9] A.A. Babaei, M. Golshan, B. Kakavandi, A heterogeneous photocatalytic sulfate radical-based oxidation process for efficient degradation of 4-chlorophenol using TiO_2 anchored on Fe oxides@carbon, Process Saf. Environ. Prot., 149 (2021) 35–47.
[10] D.J.L. Prak, E.A. Milewski, E.E. Jedlicka, A.J. Kersey, D.W. O'Sullivan, Influence of pH, temperature, salinity, and dissolved organic matter on the photolysis of 2,4-dinitrotoluene and 2,6-dinitrotoluene in seawater, Mar. Chem., 157 (2013) 233–241.
[11] J. Ge, Y. Zhang, Y.-J. Heo, S.-J. Park, Advanced design and synthesis of composite photocatalysts for the remediation of wastewater: a review, Catalysts, 9 (2019) 122, doi: 10.3390/catal9020122.
[12] A. Shokri, Degradation of 4-chlorophenol in aqueous media thru UV/persulfate method by artificial neural network and

full factorial design method, Int. J. Environ. Anal. Chem., (2020) 1–15, doi: 10.1080/03067319.2020.1791328.
[13] S. Jorfi, B. Kakavandi, H.R. Motlagh, M. Ahmadi, N. Jaafarzadeh, A novel combination of oxidative degradation for benzotriazole removal using TiO_2 loaded on $Fe^{II}Fe_2^{III}O_4$@C as an efficient activator of peroxymonosulfate, Appl. Catal., B, 219 (2017) 216–230.
[14] A. Shokri, A.H. Joshagani, Using microwave along with TiO_2 for degradation of 4-chloro-2-nitrophenol in aqueous environment, Russ. J. Appl. Chem., 89 (2016) 1985–1990.
[15] A. Shokri, K. Mahanpoor, Removal of ortho-toluidine from industrial wastewater by UV/TiO_2 process, J. Chem. Health Res, 63 (2016) 213–223.
[16] M.H. Mahmoudian, M. Fazlzadeh, M.H. Niari, A. Azari, E.C. Lima, A novel silica supported chitosan/glutaraldehyde as an efficient sorbent in solid phase extraction coupling with HPLC for the determination of Penicillin G from water and wastewater samples, Arabian J. Chem., 13 (2020) 7147–7159.
[17] A. Shokri, K. Mahanpoor, D. Soodbar, Evaluation of a modified TiO_2 (GO–B–TiO_2) photo catalyst for degradation of 4-nitrophenol in petrochemical wastewater by response surface methodology based on the central composite design, J. Environ. Chem. Eng., 4 (2016) 585–598.
[18] S. Nasseri, M.O. Borna, A. Esrafili, R.R. Kalantary, B. Kakavandi, M. Sillanpää, A. Asadi, Photocatalytic degradation of malathion using Zn^{2+}-doped TiO_2 nanoparticles: statistical analysis and optimization of operating parameters, Appl. Phys. A, 124 (2018) 1–11.
[19] M. Gebrezgiabher, G. Gebreslassie, T. Gebretsadik, G. Yeabyo, F. Elemo, Y. Bayeh, M. Thomas, W. Linert, A C-doped TiO_2/Fe_3O_4 nanocomposite for photocatalytic dye degradation under natural sunlight irradiation, J. Compos. Sci., 3 (2019) 75, doi: 10.3390/jcs3030075.
[20] M. Ismael, A review and recent advances in solar-to-hydrogen energy conversion based on photocatalytic water splitting over doped-TiO_2 nanoparticles, Solar Energy, 211 (2020) 522–546.
[21] J. Rashid, M. Barakat, Y. Ruzmanova, A. Chianese, Fe_3O_4/SiO_2/TiO_2 nanoparticles for photocatalytic degradation of 2-chlorophenol in simulated wastewater, Environ. Sci. Pollut. Res., 22 (2015) 3149–3157.
[22] J. Saien, F. Shahrezaei, Organic pollutants removal from petroleum refinery wastewater with nanotitania photocatalyst and UV light emission, Int. J. Photoenergy, 2012 (2012) 703074, doi: 10.1155/2012/703074.
[23] B.J. Rani, M. Ravina, B. Saravanakumar, G. Ravi, V. Ganesh, S. Ravichandran, R. Yuvakkumar, Ferrimagnetism in cobalt ferrite ($CoFe_2O_4$) nanoparticles, Nano-Struct. Nano-Objects, 14 (2018) 84–91.
[24] D. Greene, R. Serrano-Garcia, J. Govan, Y.K. Gun'ko, Synthesis characterization and photocatalytic studies of cobalt ferrite-silica-titania nanocomposites, Nanomaterials, 4 (2014) 331–343.
[25] K. Laohhasurayotin, S. Pookboonmee, D. Viboonratanasri, W. Kangwansupamonkon, Preparation of magnetic photo-catalyst nanoparticles—TiO_2/SiO_2/Mn–Zn ferrite—and its photocatalytic activity influenced by silica interlayer, Mater. Res. Bull., 47 (2012) 1500–1507.
[26] A. Shokri, A. Bayat, K. Mahanpoor, Employing Fenton-like process for the remediation of petrochemical wastewater through Box–Behnken design method, Desal. Water Treat, 166 (2019) 135–143.
[27] B. Mirza Hedayat, M. Noorisepehr, E. Dehghanifard, A. Esrafili, R. Norozi, Evaluation of photocatalytic degradation of 2,4-dinitrophenol from synthetic wastewater using Fe_3O_4@SiO_2@TiO_2/rGO magnetic nanoparticles, J. Mol. Liq., 264 (2018) 571–578.
[28] S. Sumiyyah, A.N. Mohd, A.H. Jawad, R. Schneider, Enhanced photocatalytic degradation of phenol by immobilized TiO_2/dye-loaded chitosan, Desal. Water Treat., 167 (2019) 190–199.
[29] S. Mortazavi-Derazkola, M. Salavati-Niasari, O. Amiri, A. Abbasi, Fabrication and characterization of Fe_3O_4@SiO_2@TiO_2@Ho nanostructures as a novel and highly efficient photocatalyst for degradation of organic pollution, J. Energy Chem., 26 (2017) 17–23.
[30] Y. Fan, C. Ma, W. Li, Y. Yin, Synthesis and properties of Fe_3O_4/SiO_2/TiO_2 nanocomposites by hydrothermal synthetic method, Mater. Sci. Semicond. Process., 15 (2012) 582–585.
[31] S. Salamat, H. Younesi, N. Bahramifar, Synthesis of magnetic core–shell Fe_3O_4@TiO_2 nanoparticles from electric arc furnace dust for photocatalytic degradation of steel mill wastewater, RSC Adv., 7 (2017) 19391–19405.
[32] A. Reghioua, D. Barkat, A.H. Jawad, A.S. Abdulhameed, M.R. Khan, Synthesis of Schiff's base magnetic crosslinked chitosan-glyoxal/ZnO/Fe_3O_4 nanoparticles for enhanced adsorption of organic dye: modeling and mechanism study, Sustainable Chem. Pharm., 20 (2021) 100379, doi: 10.1016/j.scp.2021.100379.
[33] A. Reghioua, D. Barkat, A.H. Jawad, A.S. Abdulhameed, S. Rangabhashiyam, M.R. Khan, Z.A. ALOthman, Magnetic chitosan-glutaraldehyde/zinc oxide/Fe_3O_4 nanocomposite: optimization and adsorptive mechanism of Remazol Brilliant Blue R dye removal, J. Polym. Environ., 29 (2021) 3932–3947.
[34] N.N. Abd Malek, A.H. Jawad, A.S. Abdulhameed, K. Ismail, B. Hameed, New magnetic Schiff's base-chitosan-glyoxal/fly ash/Fe_3O_4 biocomposite for the removal of anionic azo dye: an optimized process, Int. J. Biol. Macromol., 146 (2020) 530–539.
[35] A. Azari, R. Nabizadeh, A.H. Mahvi, S. Nasseri, Magnetic multi-walled carbon nanotubes-loaded alginate for treatment of industrial dye manufacturing effluent: adsorption modelling and process optimisation by central composite face-central design, Int. J. Environ. Anal. Chem., (2021) 1–21, doi: 10.1080/03067319.2021.1877279.
[36] A. Shokri, S. Karimi, Treatment of aqueous solution containing Acid red 14 using an electro peroxone process and a Box–Behnken experimental design, Arch. Hyg. Sci., 9 (2020) 48–57.
[37] M. Kermani, B. Kakavandi, M. Farzadkia, A. Esrafili, S.F. Jokandan, A. Shahsavani, Catalytic ozonation of high concentrations of catechol over TiO_2@Fe_3O_4 magnetic core-shell nanocatalyst: optimization, toxicity and degradation pathway studies, J. Cleaner Prod., 192 (2018) 597–607.
[38] S. Nasseri, M.O. Borna, A. Esrafili, R.R. Kalantary, B. Kakavandi, M. Sillanp, A. Asadi, Photocatalytic degradation of malathion using Zn^{2+}-doped TiO_2 nanoparticles: statistical analysis and optimization of operating parameters, Appl. Phys. A, 124 (2018) 175–187.
[39] K.M. Reza, A. Kurny, F. Gulshan, Parameters affecting the photocatalytic degradation of dyes using TiO_2: a review, Appl. Water Sci., 7 (2017) 1569–1578.
[40] M. Saghi, A. Shokri, A. Arastehnodeh, M. Khazaeinejad, A. Nozari, The photo degradation of methyl red in aqueous solutions by α-Fe_2O_3/SiO_2 nano-photocatalyst, J. Nanoanalysis, 5 (2018) 163–170.
[41] A.A. Babaei, M. Golshan, B. Kakavandi, A heterogeneous photocatalytic sulfate radical-based oxidation process for efficient degradation of 4-chlorophenol using TiO_2 anchored on Fe oxides@carbon, Process Saf. Environ. Prot., 147 (2021) 35–47.
[42] M. Shaban, M.R. Abukhadra, S.S. Ibrahim, M.G. Shahien, Photocatalytic degradation and photo-Fenton oxidation of Congo red dye pollutants in water using natural chromite—response surface optimization, Appl. Water Sci., 7 (2017) 4743–4756.
[43] A. Shokri, Employing UV/peroxydisulphate (PDS) activated by ferrous ion for the removal of toluene in aqueous environment: electrical consumption and kinetic study, Int. J. Environ. Anal. Chem., (2020) 1–18, doi: 10.1080/03067319.2020.1784887.
[44] S. Sepahvand, M. Bahrami, N. Fallah, Photocatalytic degradation of 2,4-DNT in simulated wastewater by magnetic $CoFe_2O_4$/SiO_2/TiO_2 nanoparticles, Environ. Sci. Pollut. Res., (2021) 1–12, doi: 10.1007/s11356-021-13690-3.